Univerzita Karlova v Praze

1. lékařská fakulta

Autoreferát disertační práce

Application of Diffusion Tensor Imaging to Brain Gray and White Matter

MUDr. Aaron Michael Rulseh

2013

Doktorské studijní programy v biomedicíně

Univerzita Karlova v Praze a Akademie věd České republiky

Obor: Zobrazovací metody v lékařství

Předseda oborové rady: Prof. MUDr. Jan Daneš, CSc.

Školicí pracoviště: Radiodiagnostické oddělení, Nemocnice Na Homolce

Školitel: Prof. MUDr. Josef Vymazal, DSc.

Disertační práce bude nejméně pět pracovních dnů před konáním obhajoby zveřejněna k nahlížení veřejnosti v tištěné podobě na Oddělení pro vědeckou činnost a zahraniční styky Děkanátu 1. lékařské fakulty.

Application of Diffusion Tensor Imaging to Brain Gray and White Matter

Abstract

In the present work we explore the gray and white matter applicability of diffusion tensor imaging (DTI). To evaluate the effect of ferritin-bound iron on gray matter contrast on DTI, we created an *in vitro* model consisting of agarose gel phantoms doped with ferritin, and validated our results *in vivo* on 29 healthy volunteer subjects 19–80 years of age in the basal ganglia. We further explored the application of DTI to amyotrophic lateral sclerosis (ALS) and multiple system atrophy (MSA); neurodegenerative diseases with gray and white matter pathophysiological components. In the ALS study, 33 patients and 30 age- and sex-matched controls were recruited, while in the MSA study, 20 probable MSA subjects (10 MSA-P, 10 MSA-C) and 20 age- and sex-matched controls were included.

We found that ferritin-bound iron makes a significant contribution to DTI indices in gray matter regions of the brain, mediated by eigenvalue repulsion. This has important implications for DTI studies targeting gray matter regions, especially in adolescence and in diseases associated with altered brain-iron load such as Huntington disease and MSA. In ALS, we found altered diffusion in the corona radiata and callosal body, and changes in R_2 in the caudate nucleus and frontal white matter. In MSA, we observed widespread white matter changes associated with a positive clinical history of cerebellar manifestations, while altered DTI metrics in the putamen were associated with a positive clinical history of Parkinsonism. The diagnostic potential of MRI in MSA may be greatly extended by applying DTI and evaluating changes in the putamen and middle cerebellar peduncle, reaching very high sensitivities and specificities.

Aplikace zobrazení difuzního tenzoru na mozkovou šedou a bílou hmotu

Abstrakt

V předložené práci zkoumáme použití zobrazení difuzního tenzoru (DTI) v mozkové šedé a bílé hmotě. K zhodnocení efektu superparamagnetického či antiferomagnetického železa na DTI kontrast v šedé hmotě jsme vytvořili in vitro model sestávající se z fantomu, vyplněného agarovým gelem s feritinem. Naše výsledky jsme poté zhodnotili na 29 zdravých dobrovolnících (39-80 let věku), a to v oblasti bazálních ganglií. Dále jsme zkoumali aplikace DTI u amyotrofické laterální sklerózy (ALS) a (mnohočetné systémové atrofie (MSA), neurodegenerativních chorob, postihujících šedou i bílou hmotu mozkovou. V ALS studii 33 pacientů a 33 zdravých dobrovolníků srovnatelných pohlavím i věkem bylo vyšetřeno, zatímco u MSA bylo zahrnuto 20 pacientů s diagnózou pravěpodobné MSA (10 s MSA-P a 10 s MSA-C) spolu s 20 zdravými dobrovolníky, srovnatelnými pohlavím a věkem.

Zjistili jsme, že železo vázané ve ferritnu signifikantně ovlivňuje skalární veličiny DTI v šedé hmotě mozkové. Tento poznatek má důležitý význam pro DTI studie, zaměřené na oblasti šedé hmoty, a to zvláště u adolescentů a u osob trpícími nemocemi se změnami ukládání železa, jako například Huntingtonova choroba či MSA. U ALS jsme nalezli změněnou difuzi v oblasti corona radiata a těla corporis callosi, a to spolu se změnami v R_2 v caput ncl. caudati a ve frontální bílé hmotě. U MSA jsme pozorovali rozsáhlé změny v bílé hmotě spojené s pozitivním klinickým obrazem mozečkové manifestace, zatímco změněné DTI hodnoty v putamen byly propojeny s pozitivním obrazem parkinsonské manifestace. Diagnostický potenciál magnetické rezonance u MSA může být významně rozšířen aplikací DTI a sledováním změn zvláště v putamen a středním cerebellárním pedunculu, kde tyto změny dosahují vysoké senzitivity a specificity.

Contents

1. Introduction

Diffusion tensor imaging (DTI) has become an invaluable tool in probing the morphological and functional characteristics of the brain in both clinical and research settings. DTI studies most often target the white matter of the brain due to its highly anisotropic structure. Factors contributing to DTI measurements in brain gray matter are not as well understood, however some investigators have proposed various mechanisms to explain their observations involving hypothetical structural changes [e.g., 1, 8, 38]. The presence of iron in the gray matter has also been suggested to affect DTI measurements [23, 34]. Healthy gray matter is characterized by age-related iron accumulation [14]. Ferritin-bound iron is the principal storage form of physiologic brain iron [52], and exhibits predominantly superparamagnetic behavior at room and body temperatures [5]. MRI is sensitive to the presence of superparamagnetic iron as it shortens T_2 relaxation time. As spin-echo echo planar imaging (SE-EPI) is T_2-weighted, the attenuation of signal in iron-rich areas of the brain can be readily appreciated in these images by visual inspection.

Neurodegenerative diseases, which may have both white and gray matter components, are often the target of DTI studies. Amyotrophic lateral sclerosis (ALS) is one such neurodegenerative disorder, which primarily affects motor neurons in the anterior horns of the spinal cord, bulbar nuclei and the

cerebral motor cortex [31], with secondary degeneration of the emerging tracts of both the central and peripheral nervous systems [20]. The diagnosis of ALS is primarily clinical and is confirmed by the demonstration of lower motor neuron loss on electromyography (EMG). Standard MR imaging of ALS patients has not revealed any unique imaging features apart from cortical atrophy, which is also characteristic of other neurodegenerative diseases. Therefore, application of DTI in conjunction with other quantitative and qualitative measures may improve the diagnostic process and advance understand of the pathogenesis.

Multiple system atrophy (MSA) is also a neurodegenerative disease that is poorly understood presents difficulty in establishing the diagnosis. Two forms of MSA are currently recognized [11]: a parkinsonian form (MSA-P, formerly striatonigral degeneration) characterized by parkinsonian features poorly responsive to L-dopa, and a cerebellar form (MSA-C, formerly olivopontocerebellar atrophy) with predominant cerebellar ataxia. The designation to one group is determined by the predominant features at evaluation. Standard MRI sequences have low sensitivity and specificity in the evaluation of MSA [6, 24–26, 28, 30, 42, 45], therefore, DTI may further improve the diagnostic process and advance our understand of the pathogenesis in MSA.

2. Hypotheses and Objectives

The primary objective of the present work was to demonstrate the applicability of DTI to the gray and white matter of the brain. We aimed to

characterize those factors that affect DTI metrics in brain gray matter, concurrent with our hypothesis that ferritin-bound iron makes an important contribution to DTI measurements in gray matter regions. To test this hypothesis, we created an *in vitro* model consisting of agarose gel phantoms doped with ferritin, and validated our results *in vivo* on healthy volunteers. We further investigated ALS and MSA for the purpose of improving the diagnostic process and advancing our understanding of the underlying pathophysiology, applying DTI as well as evaluating standard qualitative and quantitative measures.

3. Materials and Methods

Application to gray matter

A series of 40-mL agarose phantoms were constructed using a 1.1% concentration of agarose at physiologic pH (7.4). Agarose (Serva, Germany) was dissolved when boiled in a 50-mM Tris-HCL buffer (pH 7.4) in individual falcon tubes 115 mm in length and 26 mm in diameter. Ferritin was added in 5 mg iron/100 mL increments up to 50 mg iron/100 mL. One gel was left as a control and was allowed to cool without the addition of ferritin. The phantoms were positioned perpendicular to the B_0 field and scanned at 23° Celsius. Additionally, 29 volunteer subjects 19–80 years of age (14 male, 15 female; 53.2 Y $\pm$ 17 SD) were included. All volunteers were determined to be free of neurological disease.

All images were acquired on Siemens Avanto 1.5T and Siemens Trio 3T

systems (Erlangen, Germany). SE-EPI data were collected in 30 gradient directions at 1.5T (b = 1100 s/mm^2; TR = 8800 ms, TE = 98 ms; NEX = 2; PE = AP/PA; 2.2 mm isotropic) and 3T (b = 1100 s/mm^2; TR = 10100 ms, TE = 98 ms; NEX = 1; PE = AP/PA; 1.9 mm isotropic). Structural images were acquired exclude pathology. CPMG data were also acquired (32 interecho times; TR = 3000 ms; 0.9 x 0.9 x 4 mm). Data were further processed in FSL [47] and FA, MD and λ1-3 maps generated. CPMG and DTI data were coregistered, and masks placed in the caudate, putamen and globus pallidus. Proton density (PD) was calculated for each echo-time 0 per ROI. SNR was determined on a per-ROI basis by dividing mean intra-ROI signal intensity by the SD in a noise ROI, and multiplying by 0.655 to correct for the Rician distribution of noise in magnitude images [10]. ROIs were evaluated in both hemispheres and then averaged. *In vitro* SE-EPI data were corrected by applying a displacement field generated by estimating the displacement in each voxel from data acquired in opposite phase-encode directions [21]. Measurements were further performed in ImageJ viewer [27]. Statistical analyses were performed in R (www.r-project.org). The Šidak correction for multiple comparisons (D/AP procedure [41]) was applied to maintain an alpha level of 0.05 (all reported P-values are corrected unless otherwise stated). The Wilcoxon rank-sum test was used to examine gender differences.

Application in amyotrophic lateral sclerosis

Thirty-three subjects fulfilling the El-Escorial criteria [4] for clinically definite ALS were included (18 men, 15 women; 62.0 Y $\pm$ 8 SD; disease duration 3–59 months). Disease severity was assessed with the ALS Functional Rating

Scale (ALS-FRS). All subjects were further evaluated for the presence or absence of dementia by a series of neuropsychological tests [40]. Thirty healthy, age-matched volunteers (CON; 16 men, 14 women; 59.7 Y $\pm$ 10 SD), free of neurological disease, were also included.

Imaging was performed on a Siemens Symphony 1.5T System (Erlangen, Germany). CPMG was performed as above. Diffusion data were obtained in 30 gradient directions (b = 400, 1100; TR = 7900 ms; TE = 101 ms; NEX = 2, 1.25 mm isotropic). ROIs were placed in ImageJ [27] in several brain regions (frontal white matter (FWM), frontal grey matter (FGM) and posterior limb of the internal capsule (PLIC), caudate, putamen, globus pallidus). DTI was performed in 24 subjects (ALS: 9 men, 3 women; 62.97 Y $\pm$ 11 SD; CON: 9 men, 3 women; 63.22 $\pm$ 11 SD). Data were processed in FSL [47] and FA and MD maps generated. TBSS (Tract-Based Spatial Statistics, [48]) was additionally performed using an FA threshold > 0.3 and results thresholded at $P < 0.05$. The Wilcoxon two-sample test was used for intergroup comparisons using an *a priori* hypothesis of decreased R_2 in the patient group, and correction for multiple comparisons was performed.

Application in multiple system atrophy

Twenty subjects probable MSA were included (10 male, 10 female, 60.9 Y $\pm$ 7 SD), including ten MSA-P (4 male, 6 female, 62.0 Y $\pm$ 9 SD) and ten MSA-C (5 male, 5 female, 59.9 Y $\pm$ 4 SD). Demographic characteristics of the MSA group are presented in Table 3.0.1. Twenty healthy volunteer subjects (9 male, 11 female, 61.3 Y $\pm$ 7 SD) were additionally included.

Table 3.0.1: MSA Patient demographics

Sub	Sex	Age (y)	Park	Cereb	LRP	HCB	Dur (y)	Dx
01	F	59.6	−	+	−	+	4	MSA-C
02	F	69.4	+	+	−	+	2	MSA-P
03	F	63.3	+	+	+	+	3	MSA-C
04	M	65.7	+	−	+	−	2	MSA-P
05	M	58.7	+	+	+	+	5	MSA-C
06	F	49.7	+	+	+	+	4	MSA-C
07	M	68.3	+	−	+	−	2	MSA-P
08	M	65.3	+	+	+	−	10	MSA-C
09	F	80.3	+	+	+	+	3	MSA-P
10	M	61.5	+	+	+	+	6	MSA-C
11	F	55.0	+	+	+	+	8	MSA-P
12	M	62.9	−	+	−	+	2	MSA-C
13	F	60.2	−	+	−	+	5	MSA-C
14	F	56.3	+	+	+	+	2	MSA-C
15	M	59.0	+	−	+	+	3	MSA-P
16	M	55.1	+	−	+	−	5	MSA-P
17	F	53.4	+	+	+	−	2	MSA-P
18	F	53.6	+	−	+	−	1	MSA-P
19	F	60.2	+	−	+	+	6	MSA-P
20	M	61.1	−	+	+	−	2	MSA-C

Table 3.0.1: Demographic characteristics of all MSA patient participants. Parkinsonism was considered positive in the presence of bradykinesia and rigidity, while cerebellar signs were documented as positive in the presence of gait ataxia, cerebellar dysarthria, limb ataxia, or cerebellar oculomotor dysfunction. y, years; Park, Parkinsonism; Cereb, cerebellar signs; LRP, signal changes in lateral rim of the putamen; HCB, hot cross bun sign; Dur, duration; dx, diagnosis; F, female; M, male; MSA-C, multiple system atrophy, cerebellar subtype; MSA-P multiple system atrophy, parkinsonian subtype.

Imaging was performed on a Siemens Avanto 1.5T scanner (Erlangen, Germany). Standard structural images were acquired to exclude pathology in controls and to evaluate the presence/absence of radiological signs associated

with MSA (signal changes in the lateral putamen associated with the accumulation of iron and gliosis [42, 44, 53], and signal changes occurring in a cruciate pattern in the pons ("hot cross bun" sign) associated with the selective depletion of pontine neurons and myelinated transverse pontocerebellar fibers [42]). SE-EPI data were acquired in 12 gradient directions (b = 1100; TR = 8839 ms, TE = 95 ms; NEX = 2; 2.2 mm isotropic) and processed offline in FSL [47], and FA, MD, RD and $\lambda 1$ maps generated ($\lambda 3$ was additionally assessed in the basal ganglia). TBSS [48] was performed at a threshold of FA > 0.4 and results thresholded at $P < 0.05$. Automated ROI analyses were performed in the caudate, putamen, globus pallidus and middle cerebellar peduncle and further processed in R (www.r-project.org). The Šidák correction for multiple comparisons (D/AP procedure [41]) was applied to maintain an alpha level of 0.05 (all reported P-values are corrected unless otherwise stated). A one-way analysis of variance (ANOVA) test was used in the gray matter regions to test for group differences, followed by the Tukey-Kramer procedure in those regions and metrics that reached significance. The pROC package [37] was used for receiver operating characteristic (ROC) analyses.

4. Results

Application to gray matter

A linear dependence of R_2 (1/T2) on ferritin-bound iron concentration was observed in vitro at 1.5T (Figure 4.0.1a; $R^2 = 0.99$, $P < 0.001$) and at 3T

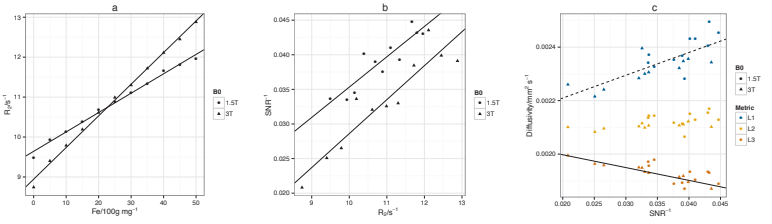

Figure 4.0.1: *In vitro* results: a) Linear dependence of R_2 on ferritin-bound iron at 1.5T and 3T, b) linear dependence of 1/SNR on R2 at 1.5T and 3T, c) eigenvalues (λ1–3) as a function of 1/SNR. Fe, ferritin-bound iron; SNR, signal-to-noise ratio.

(Figure 4.0.1a; $R^2 = 0.99$, $P < 0.001$). The relationship between SNR and R_2 was found to be reciprocal, therefore reciprocal SNR (1/SNR) was used in all further analyses to achieve linearity. 1/SNR increased linearly (SNR decreased) with increasing iron concentration at both 1.5T ($R^2 = 0.79$, $P = 0.002$) and at 3T ($R^2 = 0.84$, $P < 0.001$), and also increased linearly (SNR decreased) with increasing R_2 at 1.5T (Figure 4.0.1b; $R^2 = 0.80$, $P = 0.001$) and 3T (Figure 4.0.1b; $R^2 = 0.86$, $P < 0.001$).

In examining the linear relationship between the eigenvalues (λ1–3) and 1/SNR (Figure 4.0.1c), only the fit between λ3 and 1/SNR at 3T was significant ($R^2 = 0.92$, $P < 0.001$), although there was a trend between λ1 and 1/SNR at 3T ($R^2 = 0.49$, $P = 0.08$). Correlation between the eigenvalues and R_2 was similar (Figure 4.0.2a), with the fit between λ3 and R_2 significant at 3T ($R^2 = 0.70$, $P = 0.006$) and a trend between λ1 and R_2 at 3T ($R^2 = 0.53$, $P = 0.06$). A linear correlation was observed between FA and 1/SNR at 1.5T ($R^2 = 0.74$, $P = 0.004$) and 3T ($R^2 = 0.84$, $P < 0.001$). The fit between FA and

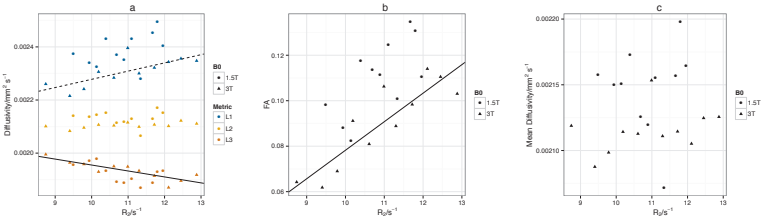

Figure 4.0.2: *In vivo* results: a) Eigenvalues (λ1–3) plotted as a function of R_2, FA as a function of R_2, MD as a function of R_2. FA, fractional anisotropy; MD, mean diffusivity.

R_2 did not reach significance at 1.5T (Figure 4.0.2b; $R^2 = 0.40$, $P = 0.17$), but was significant at 3T (Figure 4.0.2b; $R^2 = 0.76$, $P = 0.002$). No changes in MD were detected (Figure 4.0.2c).

A linear dependence of 1/SNR on R_2 was observed in vivo ($R^2 = 0.67$, $P < 0.001$). The eigenvalues decreased linearly with increasing R_2 (Figure 4.0.3a; λ1: $R^2 = 0.10$, $P = 0.03$; λ2: $R^2 = 0.36$, $P < 0.001$; λ3: $R^2 = 0.58$, $P < 0.001$), and a similar pattern was seen between the Eigenvalues and 1/SNR, although the fit with λ1 was not significant (λ1: $R^2 = 0.02$, $P = 0.56$; λ2: $R^2 = 0.17$, $P < 0.001$; λ3: $R^2 = 0.34$, $P < 0.001$). As in vitro, FA increased with increasing 1/SNR ($R^2 = 0.34$, $P < 0.001$) and R_2 (Figure 4.0.3b; $R^2 = 0.51$, $P < 0.001$), with stronger correlation between FA and R_2. MD decreased with increasing 1/SNR ($R^2 = 0.19$, $P < 0.001$) and R_2 (Figure 4.0.3c; $R^2 = 0.39$, $P < 0.001$), again with stronger correlations between MD and R_2. PD correlated only weakly with R_2 ($R^2 = 0.15$, $P = 0.003$), FA ($R^2 = 0.22$, $P < 0.001$), and λ3 ($R^2 = 0.13$, $P = 0.006$).

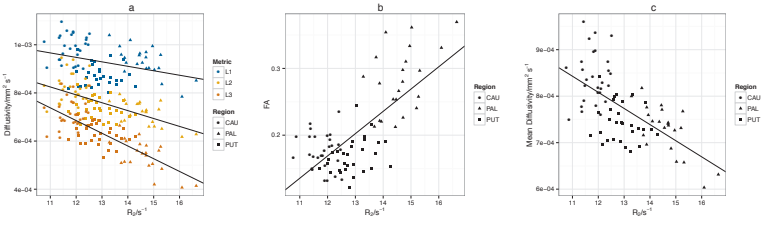

Figure 4.0.3: *In vivo* results: a) Eigenvalues (λ1–3) plotted as a function of R_2, b) linear dependence of FA on R_2, c) linear dependence of MD on R_2. FA, fractional anisotropy; MD, mean diffusivity; CAU, caudate; PUT, putamen; PAL, globus pallidus.

Application in amyotrophic lateral sclerosis

We detected significantly decreased R_2 in the head of the left caudate nucleus ($P = 0.002$, uncorrected) in ALS subjects (Table 4.0.1). Lower R_2 was also present in the deep FWM in ALS patients (left, $P = 0.002$ uncorrected; right, $P = 0.004$ uncorrected). R_2 in the FWM also correlated negatively with age in both patients and controls. No dependence of R_2 on disease duration was observed, and no relaxometric or FA/MD differences between ALS subjects and controls were detected in the PLIC. TBSS showed decreased FA in ALS patients in the bilateral corona radiata and callosal body.

Table 4.0.1: Select T_2 relaxometry results in ALS

Region	ALS	SD	Controls	SD	P-value
Head CN, L	99.7	6.4	95.6	3.4	0.002*
Head CN, R	99	7.1	96.6	4.5	0.023
FWM, L	88.8	7.8	84	4.9	0.002*
FWM, R	88.2	6.3	84.4	4.5	0.004*

Table 4.0.1: Select T_2 relaxometry results (in milliseconds) in ALS and control subjects. P-values are uncorrected, significant differences after correction for multiple comparisons are marked with an asterisk (*). ALS, amyotrophic lateral sclerosis; SD, standard deviation; L, left; R, right; CN, caudate nucleus; FWM, frontal white matter; GP, globus pallidus; Cingulate, cingulate gyrus; CST, corticospinal tract.

Application in multiple system atrophy

In MSA, TBSS showed widespread differences in RD and MD, with changes in FA and AD following but in fewer voxels (Figure 4.0.4). RD and MD were increased and FA reduced in the superior cerebellar peduncles (SCP), middle cerebellar peduncles (MCP) and inferior cerebellar peduncles (ICP) bilaterally (Figure 4.0.4a-c). Changes in RD and MD were also more widespread supratentorially, being increased throughout the corona radiata and commissural fibers bilaterally, in the body and genu of the corpus callosum in the midline, the bilateral internal and external capsules and in many subcortical areas (Figure 4.0.4a,b). Reduced FA followed a similar pattern but was observed in fewer voxels (Figure 4.0.4c).

We further explored differences between controls and the MSA-P and MSA-C diagnostic subgroups by TBSS. In MSA-P, only supratentorial differences

were observed in comparison with controls. In MSA-C, differences were similar to those between all MSA subjects and controls.

Considering the surprising result that no differences between the MSA-C and MSA-P diagnostic subgroups were detected by TBSS, we hypothesized that this negative result may be due to overlap between the patient groups. Therefore, the MSA group was reclassified according to phenotype into three subgroups: cMSA (cerebellar positive), pMSA (parkinsonian positive), and mMSA (mixed, both cerebellar and parkinsonian positive). Further TBSS analyses were conducted. In the cMSA group, we observed widespread changes similar to all MSA patients versus controls. No differences between pMSA and controls were detected by TBSS. In examining cMSA versus pMSA patients, differences were detected primarily infratentorially in RD and MD.

We additionally evaluated DTI metrics in the basal ganglia (caudate nucleus, putamen, globus pallidus). Tests were performed using different patient classifications: between the traditional MSA subgroups (MSA-C, MSA-P) and controls (traditional), and between parkinsonian-positive MSA subjects (pPOS), parkinsonian-negative MSA subjects (pNEG) and controls (phenotypic). We found significant differences in the bilateral putamen only, in $\lambda 1$, $\lambda 3$, MD and RD (see Table 4.0.1). No differences in FA in the putamen were detected. ROC analyses in those metrics reaching significance indicated that $\lambda 1$ and MD provided the best potential classification ability in the bilateral putamen under both patient classifications (Table 4.0.1). Reclassification of the data by phenotype resulted in generally greater area

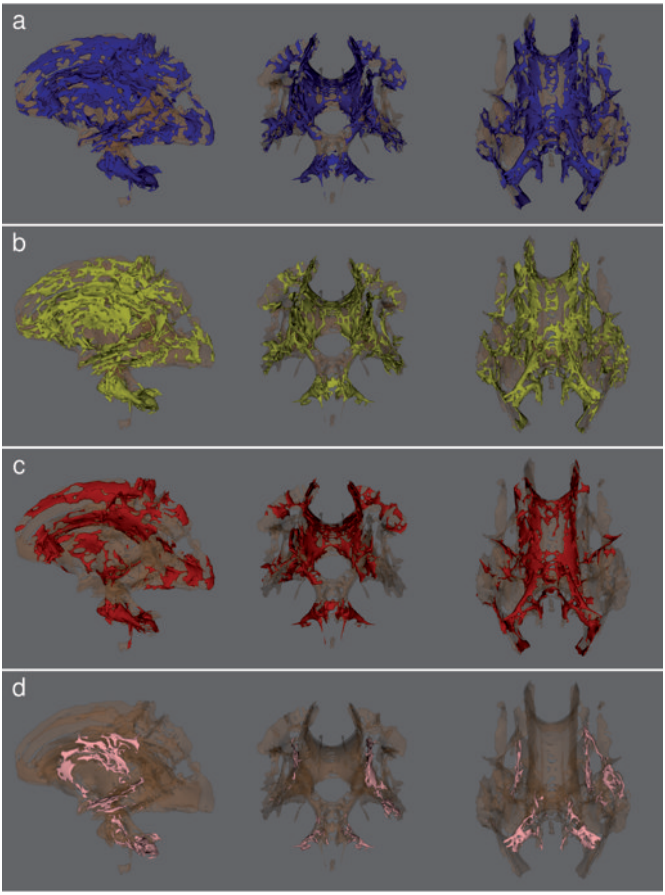

Figure 4.0.4: TBSS results: voxels demonstrating significant ($P < 0.05$) differences between all patients and controls. a) Radial diffusivity (patients > controls), b) mean diffusivity (patients > controls), c) fractional anisotropy (patients < controls), and d) axial diffusivity (patients > controls). TBSS, tract-based spatial statistics; MSA, multiple system atrophy.

Table 4.0.1: ANOVA results in the bilateral putamen

Traditional				Phenotypic			
Side	Metric	F-value	P-value	Side	Metric	F-value	P-value
L	FA	$F(2,37) = 2.7185$	$P = 0.82$	L	FA	$F(2,37) = 1.6619$	$P = 0.99$
L	$\lambda 1$	$F(2,37) = 12.636$	$P = 0.001$	L	$\lambda 1$	$F(2,37) = 10.364$	$P = 0.006$
L	$\lambda 3$	$F(2,37) = 9.3191$	$P = 0.011$	L	$\lambda 3$	$F(2,37) = 8.4826$	$P = 0.019$
L	MD	$F(2,37) = 11.674$	$P = 0.002$	L	MD	$F(2,37) = 9.9842$	$P = 0.007$
L	RD	$F(2,37) = 10.575$	$P = 0.005$	L	RD	$F(2,37) = 9.3218$	$P = 0.011$
R	FA	$F(2,37) = 2.0814$	$P = 0.96$	R	FA	$F(2,37) = 0.2823$	$P = 0.99$
R	$\lambda 1$	$F(2,37) = 15.833$	$P < 0.001$	R	$\lambda 1$	$F(2,37) = 12.451$	$P = 0.002$
R	$\lambda 3$	$F(2,37) = 11.688$	$P = 0.002$	R	$\lambda 3$	$F(2,37) = 10.993$	$P = 0.004$
R	MD	$F(2,37) = 14.196$	$P < 0.001$	R	MD	$F(2,37) = 12.153$	$P = 0.002$
R	RD	$F(2,37) = 12.786$	$P = 0.001$	R	RD	$F(2,37) = 11.543$	$P = 0.003$

Table 4.0.1: Results of ANOVA analyses of ROI data in the bilateral putamen. L, left; R, right; FA, fractional anisotropy; MD, mean diffusivity; RD, radial diffusivity

between the two ROC curves (see Table 4.0.1).

Table 4.0.1: ROC results in the bilateral putamen

Traditional				Phenotypic			
		AUC				AUC	
Side	Metric	Con vs MSA-C	Con vs MSA-P	Side	Metric	Con vs pNEG	Con vs pPOS
L	λ1	0.75	0.95	L	λ1	0.61	0.90
L	λ3	0.74	0.82	L	λ3	0.51	0.84
L	MD	0.78	0.93	L	MD	0.62	0.92
L	RD	0.80	0.89	L	RD	0.64	0.90
R	λ1	0.87	0.92	R	λ1	0.85	0.90
R	λ3	0.86	0.87	R	λ3	0.79	0.88
R	MD	0.87	0.90	R	MD	0.82	0.90
R	RD	0.87	0.87	R	RD	0.82	0.88

Table 4.0.1: Results of ROC analyses of ROI data in the bilateral putamen between patients and controls. AUC, area under curve; MSA-C, multiple system atrophy, traditional cerebellar subtype; MSA-P multiple system atrophy, traditional parkinsonian subtype; pNEG, parkinsonian-negative; pPOS, parkinsonian-positive; L, left; R, right; MD, mean diffusivity; RD, radial diffusivity.

ROC analyses in the MCP were also performed using two patient classifications: between the traditional MSA subgroups (MSA-C, MSA-P) and controls (traditional), and between cerebellar-positive MSA subjects (cPOS), cerebellar-negative MSA subjects (cNEG) and controls (phenotypic). Reclassification of the data by phenotype again resulted in generally greater area between the two ROC curves (see Table 4.0.1).

Table 4.0.1: ROC results in the MCP

Traditional				Phenotypic			
		AUC				AUC	
Side	Metric	Con vs MSA-C	Con vs MSA-P	Side	Metric	Con vs cPOS	Con vs cNEG
L	RD	0.96	0.77	L	RD	0.97	0.61
L	MD	0.92	0.78	L	MD	0.94	0.63
L	FA	0.97	0.75	L	FA	0.98	0.58
L	$\lambda 1$	0.87	0.73	L	$\lambda 1$	0.85	0.68

Table 4.0.1: Results of ROC analyses of ROI data in the bilateral MCP between patients and controls. AUC, area under curve; MSA-C, multiple system atrophy, cerebellar subtype; MSA-P multiple system atrophy, parkinsonian subtype; cPOS, cerebellar-positive MSA; cNEG, cerebellar-negative MSA; L, left; R, right; RD, radial diffusivity; MD, mean diffusivity; FA, fractional anisotropy.

We also assessed qualitative radiological signs associated with MSA that are appreciable on traditional imaging sequences; signal changes in the lateral putamen, and the hot cross bun sign in the pons (see Table 4.0.1). Traditional classification and classification by phenotype (cPOS, pPOS) were performed. In general, we observed better performance when considering MSA by phenotypic expression, the only exception being a higher negative predictive value (NPV) of the hot cross bun test in the traditional classification.

Table 4.0.1: Qualitative radiological signs

	Traditional		Phenotypic	
	BUN	RIM	BUN	RIM
Sensitivity	.80	.73	.79	.94
Specificity	.50	.33	.67	.75
PPV	.62	.57	.85	.94
NPV	.71	.50	.57	.74

Table 4.0.1: Evaluation of qualitative radiological signs typically associated with multiple system atrophy. Phenotypic classifications were cerebellar-positive MSA (cPOS) in evaluation of the BUN sign, and parkinsonian-positive (pPOS) in assessment of the RIM sign. BUN, hot cross bun sign, RIM, signal changes in the lateral rim of the putamen, PPV, positive predictive value, NPV, negative predictive value.

5. Discussion

Application to gray matter

We have shown the applicability of DTI to both gray and white matter regions of the brain. While the correlates of DTI metrics in brain white matter are relatively well understood [49–51], DTI in the gray matter is more difficult to interpret. Our *in vitro* data illustrate the isolated effect of ferritin-bound iron, mediated by iron-dependent signal attenuation. Eigenvalue repulsion with decreasing SNR has been previously reported [3, 35]. Although only changes

in λ3 were significant at 3T, there was a clear visual trend of eigenvalue repulsion that was reflected in FA changes. FA increased with increasing 1/SNR (decreasing SNR) and R_2, while MD was insensitive to these changes *in vitro*. These findings are supported by our *in vivo* data where similar correlations were observed. Linear dependencies between tensor-derived scalars and 1/SNR and R_2 were achieved in pooled data, with FA increasing and MD decreasing as 1/SNR and R_2 increased.

Certain factors must be taken into consideration when attempting to interpret differences between the *in vivo* and *in vitro* results. The *in vivo* environment is more complex, with many factors that could contribute to DTI measurements such as the presence of myelinated fibers in gray matter structures and physiological noise. Furthermore, the clustering effect of ferritin *in vivo* increases magnetic inhomogeneity [13, 52]. R_2 is also not only dependent on iron content, but is affected by several factors such as temperature, tissue density, and water content [2, 3, 35]. λ3 showed the strongest correlation with R_2 both *in vitro* and *in vivo*, seemingly the least affected by confounding factors *in vivo*. λ3 measurements within the individual nuclei followed R_2 values, while FA and MD values proved less specific. The pattern observed in FA values within the basal ganglia is in agreement with previously published data [17].

Several mechanisms have been proposed to explain DTI findings in gray matter regions, such as the loss of myelinated fibers passing through gray matter structures [9, 38], neuronal and dendrite elimination with age [16] and the targeted loss of certain dendrite connections leading to increased anisotropy [15], as well as tissue compaction and gliosis associated with aging [54]. Our results show that ferritin-bound iron makes an important contribution to DTI metrics in low-signal, isotropic, iron-rich regions, which

is an important consideration in studies examining the DTI characteristics of gray matter regions, especially in studies focused on adolescence as well as diseases associated with altered brain-iron load such as Huntington disease and MSA. Based on our *in vitro* findings, we would expect that a fifty percent increase in R_2 would result in a 75% increase in FA. This estimate is roughly in agreement with our *in vivo* observations where additional confounding factors, as discussed previously, would be expected to contributions as well.

Application to amyotrophic lateral sclerosis

We have shown T_2 relaxation rate differences in the head of caudate nucleus in ALS subjects in comparison to controls. Changes of T_2 relaxation rate in this region are of further importance as the caudate nucleus has been used as an internal reference in qualitative and quantitative studies of ALS patients [18, 19, 29]. It is interesting to note that the relaxation rate changes detected in this region were not dependent on disease duration. This suggests that decreased R_2 is already present in the earlier stages of the disease and could therefore serve as an early marker of disease activity. We also detected significantly decreased R_2 in the bilateral FWM of ALS patients compared to controls. Therefore, we recommend that FWM (as well as head of caudate nuclei) not be used as an internal reference for the assessment of increased signal intensity in various brain regions in ALS [18, 19]. Additionally, no changes were detected in the PLIC, a region suspected of signal intensity changes in ALS. Furthermore, although TBSS revealed FA changes in the corona radiata and callossal body, no differences were detected in the lower CST. Our study therefore quantitatively confirms earlier statements [7, 12]

that the relatively hyperintense signal in the internal capsule is a physiological variant and not disease related as was believed [20, 56].

Application to multiple system atrophy

We observed widespread differences in the white matter of MSA subjects in comparison to controls, reflected primarily in increased RD and MD (see Figure 4.0.4). While MD is known to be a sensitive but non-specific marker of morphological changes in the white matter, RD has been shown to correlate with myelin integrity [49, 50]. Our findings therefore lend support to the hypothesis that MSA is a primary oligodendrogliopathy.

In examining DTI differences between the MSA-P and MSA-C subgroups and controls, we observed similar differences between MSA-C subjects and controls as with all patients, and only supratentorial differences between MSA-P subjects and controls. Again, the MSA-C and MSA-P subgroups showed the greatest differences in RD and MD. These observations are not in conflict with those reported previously [22, 32, 36, 46]. Half of the patient participants in our study exhibited both cerebellar and parkinsonian manifestations, in agreement with previous studies [33, 43]. As we did not observe any differences between the MSA-C and MSA-P diagnostic subgroups by TBSS, we hypothesized that the large degree of overlap was likely responsible. We therefore reclassified our patient group by phenotype, separating those subjects with only cerebellar (cMSA) or parkinsonian manifestations (pMSA) from those with a mixed presentation. TBSS was then performed on the restructured groups.

Differences between cMSA subjects and controls by TBSS were similar to those between MSA-C and controls. To our surprise, pMSA subjects did not differ significantly from controls in any region, by any DTI metric. This may indicate an alternate pathogenesis behind the parkinsonian component of MSA. In a large series of 100 definite MSA cases, Ozawa et al. [33] reported that pathological changes in striatonigral degeneration likely begin in the substantia nigra, where neuronal cell death appears to occur independent of GCI accumulation, and concluded that other factors contribute to this phenotype. The authors did not observe any cases of pure striatonigral or olivopontocerebellar pathology (corresponding to pMSA and cMSA in the present work), likely related to the postmortem nature of the study, i.e., at the terminus of the disease process it is likely that both striatonigral and olivopontocerebellar systems are effected. Our observations in pMSA and cMSA support the hypothesis that factors other than GCI accumulation may be responsible for striatonigral degeneration. The differences in DTI metrics detected by TBSS between patients and controls were driven by the cerebellar component of the disease, i.e., by patients with a positive cerebellar phenotype, supported by the finding that the pMSA subgroup did not differ from controls.

In evaluating differences in DTI metrics in the basal ganglia between MSA subjects and controls, we explored differences between both the traditional MSA subgroups and controls, as well as between phenotypic MSA subgroups and controls. The reclassification by phenotype was performed in an attempt to increase the utility of DTI in this setting, concordant with our hypothesis that parkinsonian-positive MSA subjects (pPOS) would likely show alterations in the basal ganglia, while parkinsonian-negative MSA subjects (pNEG) would likely not. The addition of $\lambda 3$ to the analysis was made to

further clarify any diffusion changes noted, as iron accumulation in the putamen has been shown previously [53, 55], and we have shown that ferritin-bound iron results in eigenvalue repulsion [39]. We detected significant differences between the MSA-P group and others, and between the pMSA group and others, in RD, MD, $\lambda 1$ and $\lambda 3$ in the putamen only, with no differences observed in FA. Further ROC analyses were carried out to explore the classification potential of these metrics in the putamen. Similar results were seen between the MSA-P versus control and pPOS versus control tests. Performance was reduced however in the pNEG versus control tests in comparison to the MSA-C versus control tests. This reflects the transfer of parkinsonian-positive MSA-C subjects to the pPOS group when reclassified, and as their classification ability no longer contributed to the AUC, it decreased. Thus, the sensitivity and specificity improved with reclassification, as more subjects were correctly classified.

We applied similar ROC analyses to the MCP, to evaluate the diagnostic potential of this region in MSA subjects with positive cerebellar manifestations. The MCP was chosen in large part due to the robust results observed by TBSS and therefore ANOVA was not performed in this region. We again explored differences between both the traditional MSA subgroups and controls, as well as between phenotypic MSA subgroups and controls. The reclassification by phenotype was similarly performed in an attempt to increase the utility of DTI in this region, concordant with our hypothesis that cerebellar-positive MSA subjects (cPOS) would likely show alterations in the MCP, while cerebellar-negative MSA subjects (cNEG) would likely not. Similar to our results in the putamen, we observed better overall performance when the data were reclassified. The AUC in cNEG versus controls was lower than in MSA-P versus controls, again reflecting the reallocation of

classification ability driven by phenotype. Therefore, classification by phenotype improved the sensitivity and specificity of the tests, allowing more patients to be correctly classified.

As a comparison and to provide complementary diagnostic information, we also evaluated the presence or absence of radiological signs associated with MSA that are appreciable on traditional imaging sequences; signal changes in the lateral putamen, and the hot cross bun sign in the pons. In general, we observed better performance when considering MSA by phenotypic expression, the only exception being a higher NPV when considering the hot cross bun sign under the traditional classification. The reason for this paradoxically better result in the traditional classification is that one MSA-P subject with a positive cerebellar phenotype (MSA-P, cPOS) had more generalized cerebellar atrophy without an appreciable hot cross bun sign. Therefore, this subject was classified a true negative when considering the traditional classification, and as a false negative under the phenotypic classification. Thus, these two qualitative signs may not be sufficient in the diagnostic process, however, we have shown that qualitative radiological signs may serve a complementary role to the more robust DTI evaluation in MSA patients, especially when considering the disease process from a phenotypical perspective.

6. Conclusions

We have shown the effect of ferritin-bound iron on DTI metrics *in vitro*, with correlation *in vivo*. Signal attenuation on SE-EPI data due to predominantly

superparamagnetic ferritin-bound iron is reflected in increased R_2 and decreased SNR, resulting in systematic, artifactual changes in tensor-derived scalars. This effect has little consequence in brain white matter where the SNR is very high, but in low-signal regions such as the gray matter DTI metrics may be significantly affected. This observation has important implications for DTI studies targeting gray matter regions, especially in studies focused on adolescence as well as diseases associated with altered brain-iron load such as Huntington disease and MSA.

In ALS, we found only non-specific changes in DTI metrics in the brain white matter. Additionally we found decreased R_2 in the left caudate and bilateral FWM, which may aid in the diagnostic process and disqualifies these regions as internal controls in ALS studies. Furthermore, we demonstrated that the PLIC is not a reliable diagnostic marker of ALS. Considering these qualitative and quantitative measures, the evaluation of ALS subjects by MRI may be improved.

In MSA, we detected widespread changes in the brain white matter, however only in MSA subjects with a positive clinical history of cerebellar manifestations. In MSA subjects with only parkinsonian features, no alterations in DTI metrics in the white matter were detected. This has important implications in the diagnosis of MSA. However, in MSA patients with a positive clinical history of Parkinsonism, we detected significantly altered tensor-derived scalars in the bilateral putamen. These changes included increased $\lambda 3$, and considering our *in vitro* results, indicates that DTI changes in the putamen are likely driven primarily by true changes in diffusion rather than changes in local iron status. In considering these observations together, we have shown that DTI in the MCP in cerebellar-positive MSA subjects and in the putamen in parkinsonian-positive MSA subjects may

differentiate MSA from control subjects with very high accuracy, greatly improving existing methods. For this purpose, we propose the use of MD, which showed very high accuracy in all relevant tests, and is readily accessible in most commercial software packages furnished by manufacturers.

References

[1] Naama Barnea-Goraly, Vinod Menon, Mark Eckert, Leanne Tamm, Roland Bammer, Asya Karchemskiy, Christopher C. Dant, and Allan L. Reiss. White matter development during childhood and adolescence: A cross-sectional diffusion tensor imaging study. *Cereb Cortex*, 15(12): 1848 –1854, December 2005.

[2] G Bartzokis, J Mintz, D Sultzer, P Marx, J S Herzberg, C K Phelan, and S R Marder. In vivo MR evaluation of age-related increases in brain iron. *AJNR Am J Neuroradiol*, 15(6):1129–1138, June 1994.

[3] Mark E. Bastin, Paul A. Armitage, and Ian Marshall. A theoretical study of the effect of experimental noise on the measurement of anisotropy in diffusion imaging. *Magn Reson Imaging*, 16(7):773–785, September 1998.

[4] B R Brooks. El escorial world federation of neurology criteria for the diagnosis of amyotrophic lateral sclerosis. *J Neurol Sci*, 124 Suppl: 96–107, July 1994.

[5] R A Brooks, J Vymazal, R B Goldfarb, J W Bulte, and P Aisen. Relaxometry and magnetometry of ferritin. *Magn Reson Med*, 40(2): 227–235, August 1998.

[6] K Bürk, M Skalej, and J Dichgans. Pontine MRI hyperintensities ("the cross sign") are not pathognomonic for multiple system atrophy (MSA). *Mov. Disord.*, 16(3):535, May 2001.

[7] G Cheung, M J Gawel, P W Cooper, R I Farb, L C Ang, and M J Gawal. Amyotrophic lateral sclerosis: correlation of clinical and MR imaging findings. *Radiology*, 194(1):263–270, January 1995.

[8] Estela Càmara, Nils Bodammer, Antoni Rodríguez-Fornells, and Claus Tempelmann. Age-related water diffusion changes in human brain: a voxel-based approach. *Neuroimage*, 34(4):1588–1599, February 2007.

[9] Gwenaëlle Douaud, Timothy E Behrens, Cyril Poupon, Yann Cointepas, Saâd Jbabdi, Véronique Gaura, Narly Golestani, Pierre Krystkowiak, Christophe Verny, Philippe Damier, Anne-Catherine Bachoud-Lévi, Philippe Hantraye, and Philippe Remy. In vivo evidence for the selective subcortical degeneration in Huntington's disease. *Neuroimage*, 46(4):958–966, July 2009.

[10] W A Edelstein, P A Bottomley, and L M Pfeifer. A signal-to-noise calibration procedure for NMR imaging systems. *Med Phys*, 11(2): 180–185, April 1984.

[11] S Gilman, G K Wenning, P A Low, D J Brooks, C J Mathias, J Q Trojanowski, N W Wood, C Colosimo, A Dürr, C J Fowler, H Kaufmann, T Klockgether, A Lees, W Poewe, N Quinn, T Revesz, D Robertson, P Sandroni, K Seppi, and M Vidailhet. Second consensus statement on the diagnosis of multiple system atrophy. *Neurology*, 71 (9):670–676, August 2008.

[12] D S Goodin, H A Rowley, and R K Olney. Magnetic resonance imaging in amyotrophic lateral sclerosis. *Ann. Neurol.*, 23(4):418–420, April 1988.

[13] Yves Gossuin, Pierre Gillis, Robert N. Muller, and Aline Hocq. Relaxation by clustered ferritin: a model for ferritin-induced relaxation in vivo. *NMR Biomed*, 20(8):749–756, 2007.

[14] B Hallgren and P Sourander. The effect of age on the non-haemin iron in the human brain. *J Neurochem*, 3(1):41–51, October 1958.

[15] Khader M Hasan, Christopher Halphen, Michael D Boska, and Ponnada A Narayana. Diffusion tensor metrics, T2 relaxation, and volumetry of the naturally aging human caudate nuclei in healthy

young and middle-aged adults: possible implications for the neurobiology of human brain aging and disease. *Magn Reson Med*, 59 (1):7–13, January 2008.

[16] Khader M. Hasan, Christopher Halphen, Arash Kamali, Flavia M. Nelson, Jerry S. Wolinsky, and Ponnada A. Narayana. Caudate nuclei volume, diffusion tensor metrics, and T2 relaxation in healthy adults and relapsing-remitting multiple sclerosis patients: Implications to understanding gray matter degeneration. *J Magn Reson Imaging*, 29(1): 70–77, January 2009.

[17] Khader M Hasan, Indika S Walimuni, Humaira Abid, Larry A Kramer, Richard E Frye, Jack M Fletcher, and Linda Ewing-Cobbs. DTI, T2 relaxation and volumetry of the human brain corpus striatum across the lifespan. In *Proceedings of the International Society for Magnetic Resonance in Medicine*, 2010. Abstract 606.

[18] M J Hecht, F Fellner, C Fellner, M J Hilz, D Heuss, and B Neundörfer. MRI-FLAIR images of the head show corticospinal tract alterations in ALS patients more frequently than T2-, T1- and proton-density-weighted images. *J. Neurol. Sci*, 186(1-2):37–44, May 2001.

[19] Martin J Hecht, F Fellner, C Fellner, M J Hilz, B Neundörfer, and D Heuss. Hyperintense and hypointense MRI signals of the precentral gyrus and corticospinal tract in ALS: a follow-up examination including FLAIR images. *J. Neurol. Sci*, 199(1-2):59–65, July 2002.

[20] E Hofmann, G Ochs, A Pelzl, and M Warmuth-Metz. The corticospinal tract in amyotrophic lateral sclerosis: an MRI study. *Neuroradiology*, 40 (2):71–75, February 1998.

[21] Dominic Holland, Joshua M. Kuperman, and Anders M. Dale. Efficient correction of inhomogeneous static magnetic field-induced distortion in echo planar imaging. *Neuroimage*, 50(1):175–183, March 2010.

[22] Mizuki Ito, Hirohisa Watanabe, Naoki Atsuta, Jo Senda, Yoshinari Kawai, Fumiaki Tanaka, Shinji Naganawa, Hiroshi Fukatsu, and Gen Sobue. Fractional anisotropy values detect pyramidal tract involvement in multiple system atrophy. *J Neurol Sci*, 271(1-2):40–46, August 2008.

[23] Jiří Keller, Aaron M Rulseh, Michael Syka, and Josef Vymazal. Fractional anisotropy in various white and gray matter regions in adulthood: dependence on age and comparison of two DTI sequences. In *Proceedings of the International Society for Magnetic Resonance in Medicine*, 2010. Abstract 1560.

[24] E Kraft, J Schwarz, C Trenkwalder, T Vogl, T Pfluger, and W H Oertel. The combination of hypointense and hyperintense signal changes on T2-weighted magnetic resonance imaging sequences: a specific marker of multiple system atrophy? *Arch. Neurol.*, 56(2):225–228, February 1999.

[25] Eun Ah Lee, Hyung In Cho, Sam Soo Kim, and Won Yong Lee. Comparison of magnetic resonance imaging in subtypes of multiple system atrophy. *Parkinsonism Relat. Disord.*, 10(6):363–368, August 2004.

[26] Y-C Lee, C-S Liu, H-M Wu, P-S Wang, M-H Chang, and B-W Soong. The 'hot cross bun' sign in the patients with spinocerebellar ataxia. *Eur. J. Neurol.*, 16(4):513–516, April 2009.

[27] P J Magelhaes, S J Ram, and M D Abramoff. Image processing with ImageJ. *Biophotonics International*, 11(7):36–42, 2004.

[28] Luke A Massey, Caroline Micallef, Dominic C Paviour, Sean S O'Sullivan, Helen Ling, David R Williams, Constantinos Kallis, Janice L Holton, Tamas Revesz, David J Burn, Tarek Yousry, Andrew J Lees, Nick C Fox, and Hans R Jäger. Conventional magnetic resonance imaging in confirmed progressive supranuclear palsy and multiple system atrophy. *Mov. Disord.*, 27(14):1754–1762, December 2012.

[29] S Ngai, Y M Tang, L Du, and S Stuckey. Hyperintensity of the precentral gyral subcortical white matter and hypointensity of the precentral gyrus on fluid-attenuated inversion recovery: variation with age and implications for the diagnosis of amyotrophic lateral sclerosis. *AJNR Am J Neuroradiol*, 28(2):250–254, February 2007.

[30] Giuseppe Nicoletti, Francesco Fera, Francesca Condino, William Auteri, Olivier Gallo, Pierfrancesco Pugliese, Gennarina Arabia, Letterio Morgante, Paolo Barone, Mario Zappia, and Aldo Quattrone. MR imaging of middle cerebellar peduncle width: Differentiation of multiple system atrophy from parkinson disease. *Radiology*, 239(3): 825–830, June 2006.

[31] H Oba, T Araki, K Ohtomo, S Monzawa, G Uchiyama, K Koizumi, Y Nogata, K Kachi, Z Shiozawa, and M Kobayashi. Amyotrophic lateral sclerosis: T2 shortening in motor cortex at MR imaging. *Radiology*, 189(3):843–846, December 1993.

[32] Kenichi Oishi, Junya Konishi, Susumu Mori, Hiroyuki Ishihara, Hideaki Kawamitsu, Masahiko Fujii, and Fumio Kanda. Reduced fractional anisotropy in early-stage cerebellar variant of multiple system atrophy. *J Neuroimaging*, 19(2):127–131, April 2009.

[33] Tetsutaro Ozawa, Dominic Paviour, Niall P Quinn, Keith A Josephs, Hardev Sangha, Linda Kilford, Daniel G Healy, Nick W Wood, Andrew J Lees, Janice L Holton, and Tamas Revesz. The spectrum of pathological involvement of the striatonigral and olivopontocerebellar systems in multiple system atrophy: clinicopathological correlations. *Brain*, 127(Pt 12):2657–2671, December 2004.

[34] Adolf Pfefferbaum, Elfar Adalsteinsson, Torsten Rohlfing, and Edith V. Sullivan. Diffusion tensor imaging of deep gray matter brain structures: Effects of age and iron concentration. *Neurobiol Aging*, 31(3):482–493, March 2010.

[35] C Pierpaoli and P J Basser. Toward a quantitative assessment of diffusion anisotropy. *Magn Reson Med*, 36(6):893–906, December 1996.

[36] Neal Prakash, Nathan Hageman, Xue Hua, Arthur W Toga, Susan L Perlman, and Noriko Salamon. Patterns of fractional anisotropy changes in white matter of cerebellar peduncles distinguish spinocerebellar ataxia-1 from multiple system atrophy and other ataxia syndromes. *Neuroimage*, 47 Suppl 2:T72–81, August 2009.

[37] Xavier Robin, Natacha Turck, Alexandre Hainard, Natalia Tiberti, Frédérique Lisacek, Jean-Charles Sanchez, and Markus Müller. pROC: an open-source package for R and S+ to analyze and compare ROC curves. *BMC Bioinformatics*, 12(1):77, March 2011.

[38] H. Diana Rosas, David S. Tuch, Nathanael D. Hevelone, Alexandra K. Zaleta, Mark Vangel, Steven M. Hersch, and David H. Salat. Diffusion tensor imaging in presymptomatic and early Huntington's disease: Selective white matter pathology and its relationship to clinical measures. *Mov Disord.*, 21(9):1317–1325, September 2006.

[39] Aaron M Rulseh, Jiří Keller, Jaroslav Tintěra, Milan Kožíšek, and Josef Vymazal. Chasing shadows: What determines DTI metrics in gray matter regions? An in vitro and in vivo study. *J Magn Reson Imaging*, February 2013. doi: 10.1002/jmri.24065.

[40] R Rusina, P Ridzon, P Kulisťák, O Keller, A Bartos, M Buncová, L Fialová, F Koukolík, and R Matej. Relationship between ALS and the degree of cognitive impairment, markers of neurodegeneration and predictors for poor outcome. a prospective study. *Eur. J. Neurol.*, 17(1): 23–30, January 2010.

[41] A J Sankoh, M F Huque, and S D Dubey. Some comments on frequently used multiple endpoint adjustment methods in clinical trials. *Stat Med*, 16(22):2529–2542, November 1997.

[42] A. Schrag, D. Kingsley, C. Phatouros, C. J. Mathias, A. J. Lees, S. E. Daniel, and N. P. Quinn. Clinical usefulness of magnetic resonance imaging in multiple system atrophy. *J Neurol Neurosurg Psychiatry*, 65 (1):65–71, July 1998.

[43] A Schrag, C D Good, K Miszkiel, H R Morris, C J Mathias, A J Lees, and N P Quinn. Differentiation of atypical parkinsonian syndromes with routine MRI. *Neurology*, 54(3):697–702, February 2000.

[44] J Schwarz, S Weis, E Kraft, K Tatsch, O Bandmann, P Mehraein, T Vogl, and W H Oertel. Signal changes on MRI and increases in reactive microgliosis, astrogliosis, and iron in the putamen of two patients with multiple system atrophy. *J Neurol Neurosurg Psychiatry*, 60 (1):98–101, January 1996.

[45] Klaus Seppi, Michael F.H. Schocke, Katherina J. Mair, Regina Esterhammer, Christoph Scherfler, Felix Geser, Christian Kremser, Sylvia Boesch, Werner Jaschke, Werner Poewe, and Gregor K. Wenning. Progression of putaminal degeneration in multiple system atrophy: A serial diffusion MR study. *Neuroimage*, 31(1):240–245, May 2006.

[46] Kensuke Shiga, Kei Yamada, Kenji Yoshikawa, Toshiki Mizuno, Tsuneo Nishimura, and Masanori Nakagawa. Local tissue anisotropy decreases in cerebellopetal fibers and pyramidal tract in multiple system atrophy. *J Neurol*, 252(5):589–596, May 2005.

[47] Stephen M Smith, Mark Jenkinson, Mark W Woolrich, Christian F Beckmann, Timothy E J Behrens, Heidi Johansen-Berg, Peter R Bannister, Marilena De Luca, Ivana Drobnjak, David E Flitney, Rami K Niazy, James Saunders, John Vickers, Yongyue Zhang, Nicola De Stefano, J Michael Brady, and Paul M Matthews. Advances in functional and structural MR image analysis and implementation as FSL. *Neuroimage*, 23 Suppl 1:S208–219, 2004.

[48] Stephen M Smith, Mark Jenkinson, Heidi Johansen-Berg, Daniel Rueckert, Thomas E Nichols, Clare E Mackay, Kate E Watkins, Olga

Ciccarelli, M Zaheer Cader, Paul M Matthews, and Timothy E J Behrens. Tract-based spatial statistics: voxelwise analysis of multi-subject diffusion data. *Neuroimage*, 31(4):1487–1505, July 2006.

[49] Sheng-Kwei Song, Shu-Wei Sun, Michael J Ramsbottom, Chen Chang, John Russell, and Anne H Cross. Dysmyelination revealed through MRI as increased radial (but unchanged axial) diffusion of water. *Neuroimage*, 17(3):1429–1436, November 2002.

[50] Sheng-Kwei Song, Shu-Wei Sun, Won-Kyu Ju, Shiow-Jiuan Lin, Anne H Cross, and Arthur H Neufeld. Diffusion tensor imaging detects and differentiates axon and myelin degeneration in mouse optic nerve after retinal ischemia. *Neuroimage*, 20(3):1714–1722, November 2003.

[51] Sheng-Kwei Song, Jun Yoshino, Tuan Q Le, Shiow-Jiuan Lin, Shu-Wei Sun, Anne H Cross, and Regina C Armstrong. Demyelination increases radial diffusivity in corpus callosum of mouse brain. *Neuroimage*, 26 (1):132–140, May 2005.

[52] J Vymazal, R A Brooks, C Baumgarner, V Tran, D Katz, J W Bulte, R Bauminger, and G Di Chiro. The relation between brain iron and NMR relaxation times: an in vitro study. *Magn Reson Med*, 35(1): 56–61, January 1996.

[53] J Vymazal, A Righini, R A Brooks, M Canesi, C Mariani, M Leonardi, and G Pezzoli. T1 and T2 in the brain of healthy subjects, patients with Parkinson disease, and patients with multiple system atrophy: relation to iron content. *Radiology*, 211(2):489–495, May 1999.

[54] Q. Wang, X. Xu, and M. Zhang. Normal aging in the basal ganglia evaluated by eigenvalues of diffusion tensor imaging. *AJNR Am J Neuroradiol*, 31(3):516–520, March 2010.

[55] Y Wang, S R Butros, X Shuai, Y Dai, C Chen, M Liu, E M Haacke, J Hu, and H Xu. Different iron-deposition patterns of multiple system atrophy with predominant parkinsonism and idiopathetic Parkinson

diseases demonstrated by phase-corrected susceptibility-weighted imaging. *AJNR Am J Neuroradiol*, 33(2):266–273, February 2012.

[56] A Yagishita, I Nakano, M Oda, and A Hirano. Location of the corticospinal tract in the internal capsule at MR imaging. *Radiology*, 191(2):455–460, May 1994.